Citrulline protects against LPS-induced acute lung injury by inhibiting ROS/NLRP3-dependent pyroptosis and apoptosis via the Nrf2 signaling pathway

YAO XUE[1*], YUNQIAN ZHANG[2*], LI CHEN[3], YAN WANG[2], ZHOU LV[2], LI-QIAO YANG[2] and SIYUAN LI[2]

[1]Department of Anesthesiology, The Affiliated Shenmu Hospital of Northwest University, Shenmu, Shaanxi 719300; [2]Department of Anesthesiology and Surgical Intensive Care Unit, Xinhua Hospital Affiliated to Shanghai Jiao Tong University School of Medicine, Shanghai 200092; [3]Department of Anesthesiology, Suqian Hospital of Nanjing Drum-Tower Hospital Group, Suqian, Jiangsu 223865, P.R. China

Received April 9, 2022; Accepted July 29, 2022

DOI: 10.3892/etm.2022.11569

Abstract. Acute lung injury (ALI) is a common complication in patients with sepsis and is accompanied by high mortality. The present study aimed to investigate if the organic compound citrulline has a protective against lipopolysaccharide (LPS)-stimulated ALI and its potential mechanisms. ALI was induced in mice by intraperitoneal (i.p.) injection of LPS (10 mg/kg). Citrulline (1 g/kg/day) was administrated i.p. 7 days prior to LPS injection. Mouse lung vascular endothelial cells (MLVECs) were divided into five groups: Control, LPS, LPS + Cit, LPS + N-acetyl-L-cysteine (NAC) and LPS + Cit + ML385. Lung injury was determined by morphology changes. Apoptosis and pyroptosis were detected using western blot analysis and immunofluorescence. The present results indicated that citrulline can significantly attenuate ALI. Citrulline pretreatment decreased the expression of NOD-, LRR- and pyrin domain-containing protein 3 (NLRP3) inflammasome and decreased pyroptosis and apoptosis. Intervention with the total reactive oxygen species (ROS) scavenger N-acetyl-L-cysteine attenuated NLRP3 inflammasome-associated pyroptosis and apoptosis in LPS-treated MLVECs. Citrulline pretreatment inhibited pyroptotic cell death and apoptosis induced by LPS. Citrulline decreased accumulation of intracellular ROS and activated the nuclear factor erythroid 2-related factor 2 (Nrf2) signaling pathway. Furthermore, the Nrf2 inhibitor ML385 reversed ROS generation, NLRP3 inflammasome-mediated pyroptosis and apoptosis suppressed by citrulline. In summary, the present data demonstrated that citrulline may confer protection against ALI via inhibition of ROS/NLRP3 inflammasome-dependent pyroptosis and apoptosis via the Nrf2 signaling pathway.

Correspondence to: Dr Li-Qiao Yang or Dr Siyuan Li, Department of Anesthesiology and Surgical Intensive Care Unit, Xinhua Hospital Affiliated to Shanghai Jiao Tong University School of Medicine, 1665 Kongjiang Road, Shanghai 200092, P.R. China
E-mail: yangliqiao@xinhuamed.com.cn
E-mail: lisiyuan@xinhuamed.com.cn

*Contributed equally

Key words: citrulline, NOD-, LRR- and pyrin domain-containing protein 3 inflammasome, pyroptosis, apoptosis, nuclear factor erythroid 2-related factor 2

Introduction

Acute lung injury (ALI) or acute respiratory distress syndrome is a common complication resulting from multiple pathogeneses, including sepsis, and is accompanied by high mortality of ~40% (1). Lipopolysaccharide (LPS) is a primary component derived from Gram-negative bacteria and is used to induce lung injury (2). Administration of LPS leads to imbalance of the alveolar capillary system, resulting in endothelial barrier disruption and neutrophil accumulation in lung (3,4). Inhibition of inflammation and oxidative products induced by LPS may be a potential target against lung injury (5).

The NOD-, LRR- and pyrin domain-containing protein 3 (NLRP3) inflammasome is a key component of the innate immune system, consisting of a nucleotide-binding domain, an apoptosis-associated speck-like protein (ASC) and pro-caspase-1 (6). Once activated, caspase-1 and gasdermin D (GSDMD) are cleaved by NLRP3, followed by the release of a large number of inflammatory factors induced by pyroptosis, which causes a severe inflammatory cascade (7,8).

NLRP3 has been reported to be involved in a variety of systemic diseases, including ALI (9). Notably, pyroptosis induced by NLRP3 is involved in pathogenesis of diverse lung injury models (10,11). Activation of the NLRP3 signaling pathway leads to apoptosis in pulmonary injury (12,13). The generation of reactive oxygen species (ROS) is one of several molecular mechanisms involved in the activation of the NLRP3 inflammasome (14). A previous study observed that an elevated inflammatory response is accompanied by increased levels of ROS, which leads to oxidative damage in lung parenchymal cells in ALI (15).

Nuclear factor erythroid-2 related factor 2 (Nrf2) is a promising therapeutic strategy against oxidative stress and inflammation (16,17). When oxidative stress occurs, Nrf2 enters the nucleus and activates certain cytoprotective genes, such as heme oxygenase-1 (HO-1) and NAD(P)H quinone dehydrogenase 1 (18). A previous study showed that Nrf2 inhibits activation of the NLRP3 inflammasome (19), thus suggesting a potential beneficial effect of Nrf2 on the pathogenesis of ALI.

Citrulline (Cit) is a non-essential amino acid produced by humans and it is also present in certain foods, such as watermelon (20). Supplementation of Cit has been shown to be beneficial in regulating insulin sensitivity, neurological function and the cardiovascular system (21). Grisafi *et al* (22) showed that Cit protects against oxygen-induced pulmonary damage by improving alveolar and vascular growth. The present study aimed to elucidate if Cit exerts a beneficial effect on LPS-stimulated ALI and LPS-treated mouse pulmonary vascular endothelial cells. It was hypothesized that Cit may inhibit pyroptosis and apoptosis mediated by the NLRP3 inflammasome, as well as decrease oxidative stress via activation of Nrf2, thereby protecting against LPS-induced ALI.

Materials and methods

Animals and ALI model. The animal experiments were performed based on the guidance for the Care and Use of Laboratory Animals (National Institutes of Health) (23). All studies were performed between June 2020 and February 2022 and were approved by the Animal Ethics Committee of Xinhua Hospital Affiliated to Shanghai Jiaotong University, School of Medicine, Shanghai, China (approval no. XHEC-NSFC-2020-038). For *in vivo* experiments, a total of 36 male mice (age, 4-6-weeks, Institute of Cancer Research) weighing 20-25 g were housed at 22-25˚C with 12/12-h day/night cycle, humidity of 50-60% and free access to food and water at specific-pathogen-free grade, were randomly divided into three groups: Control, LPS and LPS + Cit (n=12/group). In each group, one set of mice (n=6/group) was used for histological analysis, while a second set (n=6/group) was used to analyze bronchoalveolar lavage fluid (BALF). For the *in vitro* experiments, primary pulmonary endothelial cells were isolated from 20 additional male mice (age 3 weeks, weight, 15 g, Shanghai Jihui Laboratory Animal Care Co., Ltd.). These mice were assigned to five groups: Control, LPS, LPS + Cit, LPS + N-acetyl-L-cysteine (NAC; 5 mM) and LPS + Cit + ML385 (5 μM; n=4/group). Control mice were intraperitoneally (i.p.) injected with saline for 6 h. LPS group: Mice were i.p. injected with LPS (10 mg/kg; Sigma-Aldrich; Merck KGaA) for 6 h. LPS + Cit Cit (MedChemExpress) was i.p. injected at a dose of 1 g/kg once daily for 1 week, followed by i.p. injected with LPS for 6 h. Lung tissue was collected following treatment. All mice were humanely sacrificed by CO_2 inhalation (May 2021) using a gradual displacement of 30-70% of the chamber volume/min when they met the following criteria: Loss of body weight >20%, difficulty breathing and sharp decrease in body temperature (24). Absence of movement and breathing, as well as presence of cardiac arrest and pupil dilation for 5 min, was used to confirm death.

Histological analysis and lung injury evaluation. Left lung lobe samples were collected, fixed with 4% paraformaldehyde at room temperature for 1 day and lung tissue was cut into 5-μm thick slices, followed by staining with hematoxylin for 5-10 min at room temperature and eosin (Beyotime Institute of Biotechnology) for 1-2 min at room temperature. Images were recorded using a light microscope (Olympus Corporation). Lung morphometry and injury analysis were scored by two independent pathologists blinded to the treatment strategy based on inflammatory infiltration and thickness of the alveolar wall. A tissue injury scoring system was implemented as follows: 0, no injury; 1, slight; 2, mild; 3, moderate; 4, moderate-to-severe and 5, severe inflammatory injury (25).

Lung wet/dry (W/D) weight ratio. Pulmonary edema index was estimated by calculating pulmonary W/D weight ratio. The fresh upper left lung lobe was isolated, weighed and dried at 65˚C for 48 h in an oven. The dry weight was determined and the W/D ratio calculated.

Preparation of BALF. Following anesthesia with i.p. 100 mg/kg ketamine and 10 mg/kg xylazine, BALF was isolated from mice via a tracheal tube by infusing 1 ml chilled PBS three times. Following collection, mice were euthanized via CO_2 inhalation. BALF was centrifuged at 500 x g for 10 min at 4˚C and the cell precipitate was resuspended in 200 μl PBS. Cell counting was performed manually under a 40x magnification using a light microscope and total protein concentration in the BALF supernatant was determined using commercial kits (Enhanced BCA Protein Assay kit; cat no. P0009; Beyotime Institute of Biotechnology).

ELISA. Lung tissue specimens (100 mg each) were homogenized in PBS containing a protease inhibitor cocktail (cat no. P9599; Sigma-Aldrich; Merck KGaA). Supernatant was obtained via centrifugation at 1,000 x g for 10 min at 4˚C. IL-1β and IL-18 concentration in the lung tissue was measured using commercial ELISA kits for IL-1β (Mouse IL-1β/IL-1F2 Quantikine ELISA; cat no. MLB00C; R&D System, Inc.) and IL-18 (Mouse IL-18/IL-1F4 ELISA; cat no. 7625; R&D Systems, Inc.) according to the manufacturer's instructions.

Apoptosis detection. TUNEL detection was used to examine apoptosis in lung tissue. Lung tissues were fixed and embedded as aforementioned. Paraffin-embedded 5-μm sections of lung tissue were rehydrated and antigen retrieval was performed by boiling in citrate buffer (pH=6.0). TUNEL staining was conducted at room temperature for 1 h according to the manufacturer's instructions (One Step TUNEL Apoptosis Assay kit; cat. no. C1090; Beyotime Institute of Biotechnology). Finally, nuclei were counterstained with DAPI (1 μg/ml) at room temperature for 2 h. The stained tissue was observed under a fluorescence microscope (magnification, x20; Nikon Corporation).

Isolation and treatment of mouse lung vascular endothelial cells (MLVECs). MLVECs were isolated as previously described (26). Briefly, peripheral and subpleural tissue was cut into small pieces (1-mm^3) and tissue fragments were placed into 60-mm cell culture dishes. DMEM (Gibco;

Thermo Fisher Scientific, Inc.) supplemented with 20% fetal bovine serum (FBS; Gibco; Thermo Fisher Scientific, Inc.) was added as culture medium. Following 48 h incubation at 37˚C, the tissue was removed and MLVECs were cultured in DMEM supplemented with 10% FBS (Gibco) and 0.01% ampicillin/streptomycin (Gibco; Thermo Fisher Scientific, Inc.) at 37˚C with 5% CO_2. MLVECs were characterized by their cobblestone morphology and stained with factor VIII-related antigen (cat. no. sc-53466, 1:100, Santa Cruz Biotechnology, Inc.) at 4˚C for one night as previously described (27). Cells after 3-4 passages were used in subsequent experiments.

Immunofluorescence assay. Lung tissue (5-μm sections) were deparaffinized in xylene and rehydrated with graded ethanol. For antigen retrieval, sections were boiled in citrate buffer (pH=6.0). Following treatment with 5% bovine serum albumin (BSA; cat. no. A8010; Beijing Solarbio Science & Technology Co., Ltd.) for 30 min at room temperature, the slices were incubated with F4/80 antibody (1:300; cat. no. GB11027; Servicebio Technology Co., Ltd.) overnight at 4˚C followed by incubation with cyanine 3-labeled goat anti-rabbit secondary antibody (1:300; cat. no. GB21303, Servicebio Technology Co., Ltd.). MLVECs were fixed in 4% paraformaldehyde at room temperature for 10 min, treated with 5% BSA for 30 min at room temperature and incubated with anti-Nrf2 primary antibody (1:200; cat. no. bs-1074R; BIOSS Biotech Co., Ltd.) at 4˚C overnight followed by incubation with FITC-labeled goat anti-rabbit secondary antibody (1:300; cat. no. GB22303; Servicebio Technology Co., Ltd.). Cell nuclei were stained with DAPI (1 μg/ml, Beyotime Institute of Biotechnology) at room temperature for 2 h. Images were obtained using a Nikon fluorescence microscope (magnification, x20; Nikon Corporation).

ROS measurement. The fluorescence probe 2',7'-dichlorofluorescein diacetate (DCFH-DA; cat. no. S0033S; Beyotime Institute of Biotechnology) was used to monitor the accumulation of intracellular ROS. Following treatment with LPS, LPS + Cit or LPS + Cit + ML385 for 6 h, MLVECs were incubated with DCFH-DA (10 μM) at 37˚C for 30 min, followed by washing twice with PBS. Images were collected using a Nikon fluorescence microscope (magnification, x20; Nikon Corporation).

Western blotting. Lung tissue or MLVECs were homogenized in cold RIPA buffer (cat. no. P0013; Beyotime Institute of Biotechnology) containing proteinase and phosphatase inhibitor cocktail (Roche Diagnostics) by a mechanical homogenizer. Following centrifugation at 1,000 x g and 4˚C for 10 min, the supernatant was collected. The total protein was quantified using a bicinchoninic acid assay kit (Beyotime Institute of Biotechnology). Protein (40 μg/lane) was separated by SDS-PAGE using 10 or 12.5% SDS-PAGE Gel Fast Preparation kits (cat. no. PG212, cat. no. PG213; Epizyme, Inc.) and transferred onto PVDF membranes. Subsequently, the membranes were blocked with 5% skimmed milk at room temperature for 2 h. Membranes were incubated with primary antibodies against NLRP3 (cat. no. 15101S, 1:1,000; Cell Signaling Technology, Inc.), GSDMD (1:500; cat. no. ab155233; Abcam), caspase-1 (cat. no. A0964; 1:1,000; ABclonal Biotech Co., Ltd.), Bcl-2 (cat. no. ab32124; 1:1,000; Abcam), Bax (cat. no. ab182733; 1:1000, Abcam) and β-actin loading control (cat. no. A1978, 1:3,000; Sigma-Aldrich; Merck KGaA) overnight at 4˚C. Following incubation with primary antibodies, the membranes were incubated with secondary HRP-conjugated Affinipure Goat Anti-Rabbit (1:5,000; cat. no. SA00001-2; ProteinTech Group, Inc.) and anti-Mouse IgG (1:5,000; cat. no. SA00001-1; ProteinTech Group, Inc.) for 1 h at room temperature. An enhanced chemiluminescence solution (cat. no. BL523A; Hefei Labgic Technology Co., Ltd.) was used to visualize the immunoblots. Finally, the protein bands were semi-quantified using ImageJ software (V1.4.3.67; National Institutes of Health) and normalized to β-actin.

Reverse transcription-quantitative PCR (RT-qPCR). TRIzol® reagent (Thermo Fisher Scientific, Inc.) was used to extract total RNA from lung tissue and MLVECs, according to the manufacturer's protocol. Total RNA was reverse-transcribed into cDNA using the One Step PrimeScript™ RT-PCR kit (cat. no. RR064A; Takara Biomedical Technology Co., Ltd.), according to the manufacturer's protocol. qPCR was performed using the ChamQ Universal SYBR qPCR Master Mix (Vazyme Biotech Co., Ltd.), according to the manufacturer's protocol. The amplification was performed using a Step One Plus system (Applied Biosystems; Thermo Fisher Scientific, Inc.) and the following thermocycling conditions: Initial denaturation at 95˚C for 10 min, followed by 40 cycles of 95˚C for 15 sec, 60˚C for 30 sec and 72˚C for 30 sec and final extension at 72˚C for 5 min. The following primer pairs were used: NLRP3 forward, 5'-TCTGACCTCTGTGCTCAAAACCAAC-3' and reverse, 5'-TGAGGTGAGGCTGCAGTTGTTAAT-3'; ASC forward, 5'-ACTCATTGCCAGGGTCACAGAAGTG-3' and reverse, 5'-GCTTCCTCATCTTGTCTTGGCTGGT-3'; Nrf2 forward, 5'-CAGTCTTCACCACCCCTGAT-3' and reverse, 5'-CAGTGAGGGGATCGATGAGT-3'; HO-1 forward, 5'-AGAGGCTAAGACCGCCTTCC-3' and reverse, 5'-TCTGACGAAGTGACGCCATC-3' and β-actin forward, 5'-TGTATGCCTCTGGTCGTAC and reverse, 3'-TGATGTCACGCACGATTTCC-3'. The relative mRNA expression levels were quantified using the $2^{-\Delta\Delta Cq}$ method and normalized to internal reference gene β-actin (28).

Statistical analysis. Statistical analysis was performed using SPSS Statistics V22.0 (IBM Corp.). Data are presented as the mean ± standard error of the mean. All experiments were performed at least three times. One-way ANOVA followed by Bonferroni's post hoc test was used to compare multiple groups. Lung injury score was evaluated using Kruskal-Wallis followed by Dunn's test. $P<0.05$ was considered to indicate a statistically significant difference.

Results

Effect of Cit on LPS-induced lung injury. To study the effect of Cit on LPS-induced lung injury, total cell count and protein concentration in BALF of mice were measured to determine changes in lung vascular permeability. Total cell count and protein concentration in BALF were significantly greater in the LPS group than in the control group, indicating notable lung injury caused by treatment with LPS ($P<0.01$; Fig. 1A and B). On the other hand, the effect of LPS treatment was partially inhibited by pretreatment with Cit (Fig. 1A and B). In addition,

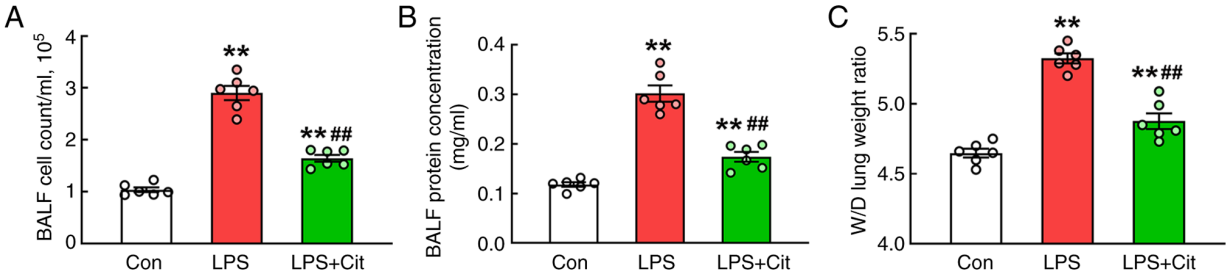

Figure 1. Effect of Cit on LPS-induced lung injury. (A) Cell count and (B) protein concentration in BALF. (C) Lung W/D ratio. Data are presented as the mean ± standard error of the mean (n=6). **P<0.01 vs. con; $^{\#\#}$P<0.01 vs. LPS. LPS, lipopolysaccharide; Con, control; Cit, citrulline; BALF, bronchoalveolar lavage fluid; W/D, wet/dry.

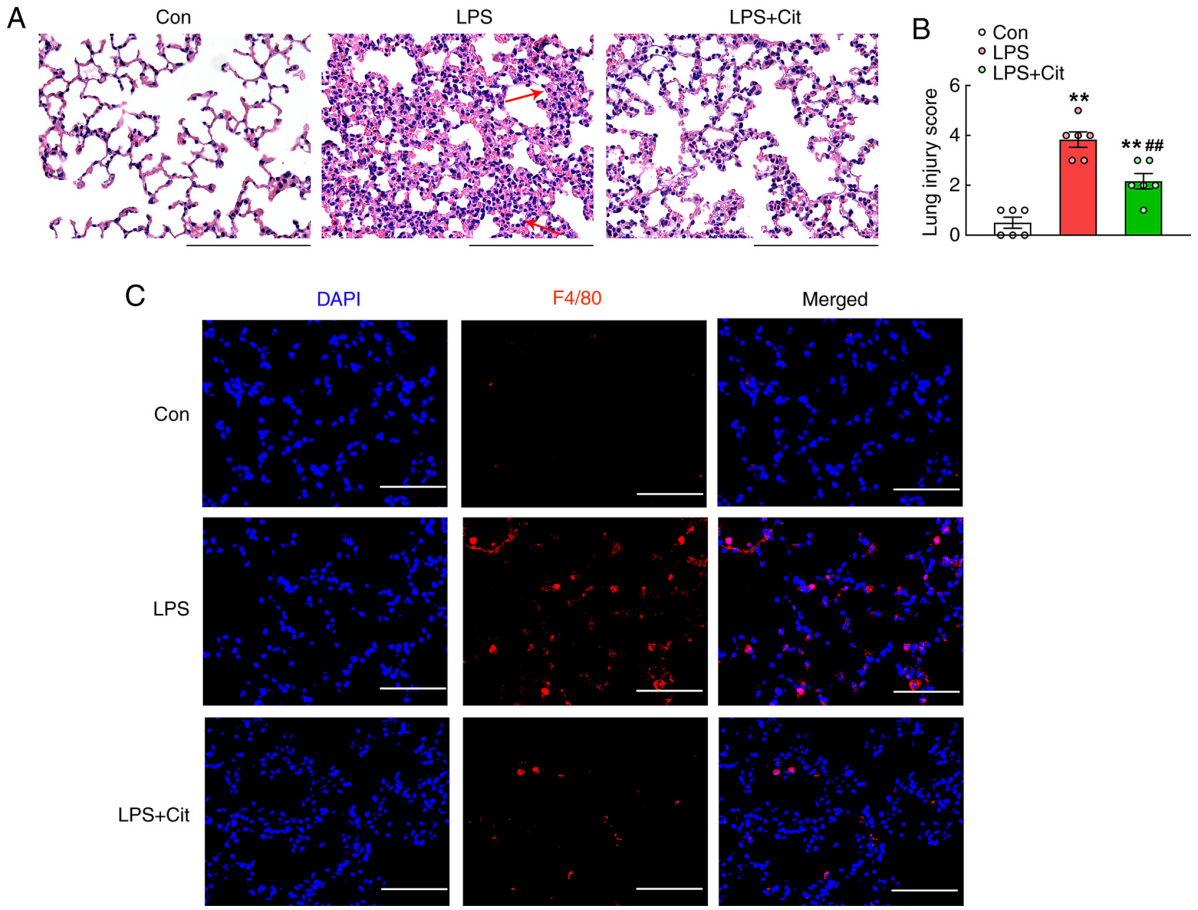

Figure 2. Effect of Cit on LPS-induced pulmonary inflammatory changes. (A) Representative histological changes of lung tissue. Scale bar, 100 μm. (B) Score representing the degree of lung injury. Data are expressed as the mean ± standard error of the mean (n=6). **P<0.01 vs. con; $^{\#\#}$P<0.01 vs. LPS. Arrows indicate inflammatory infiltration and thickened alveolar wall. (C) Representative macrophage infiltration shown as F4/80-positive cells. Sections were stained with primary antibodies against F4/80 (red), while the nucleus was stained with DAPI (blue). Scale bar, 100 μm. LPS, lipopolysaccharide; Con, control; Cit, citrulline.

the increase in the lung W/D ratio induced by LPS was significantly attenuated by pretreatment with Cit (Fig. 1C).

Effect of Cit on LPS-induced lung inflammatory changes. The effect of pretreatment with Cit on lung injury induced by LPS was investigated by histopathological analysis. The lung tissue in the LPS group showed a lung injury score significantly greater than that in the control, showing distinct pathological injury, including neutrophil accumulation, interstitial edema and alveolar wall damage (Fig. 2A and B). Lung injury score in the LPS + Cit group was significantly lower than that in the LPS group (Fig. 2B) but greater than that in the control (Fig. 2B). Mice in the LPS group showed severe infiltration of F4/80$^+$ macrophages, while there was a decreasing tendency in LPS + Cit mice (Fig. 2C), indicating the anti-inflammatory effect of Cit.

Cit protects against LPS-induced activation of the NLRP3 inflammasome. Yang *et al* (29) showed that NLRP3 inflammasome activation participates in LPS-stimulated lung injury.

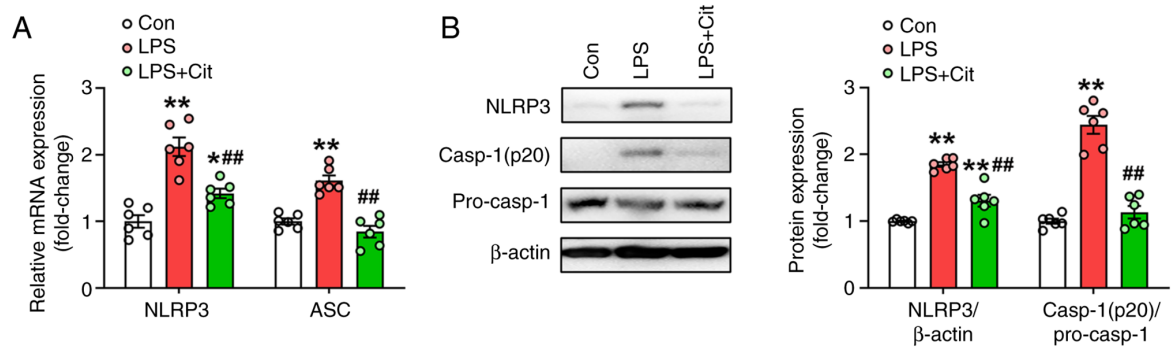

Figure 3. Cit protects against LPS-induced activation of the NLRP3 inflammasome. (A) Relative mRNA expression of NLRP3 and ASC. (B) NLRP3 and casp-1 p20 fragment expression levels determined by western blotting. Relative densitometry of NLRP3/β-actin and casp-1 p20/pro-casp-1 ratio is shown. Data are presented as the mean ± standard error of the mean (n=6). *P<0.05 and **P<0.01 vs. con; $^{\#\#}$P<0.01 vs. LPS. LPS, lipopolysaccharide; NLRP3, NOD-, LRR- and pyrin domain-containing protein 3; Con, control; Cit, citrulline; casp, caspase; ASC, apoptosis-associated speck-like protein.

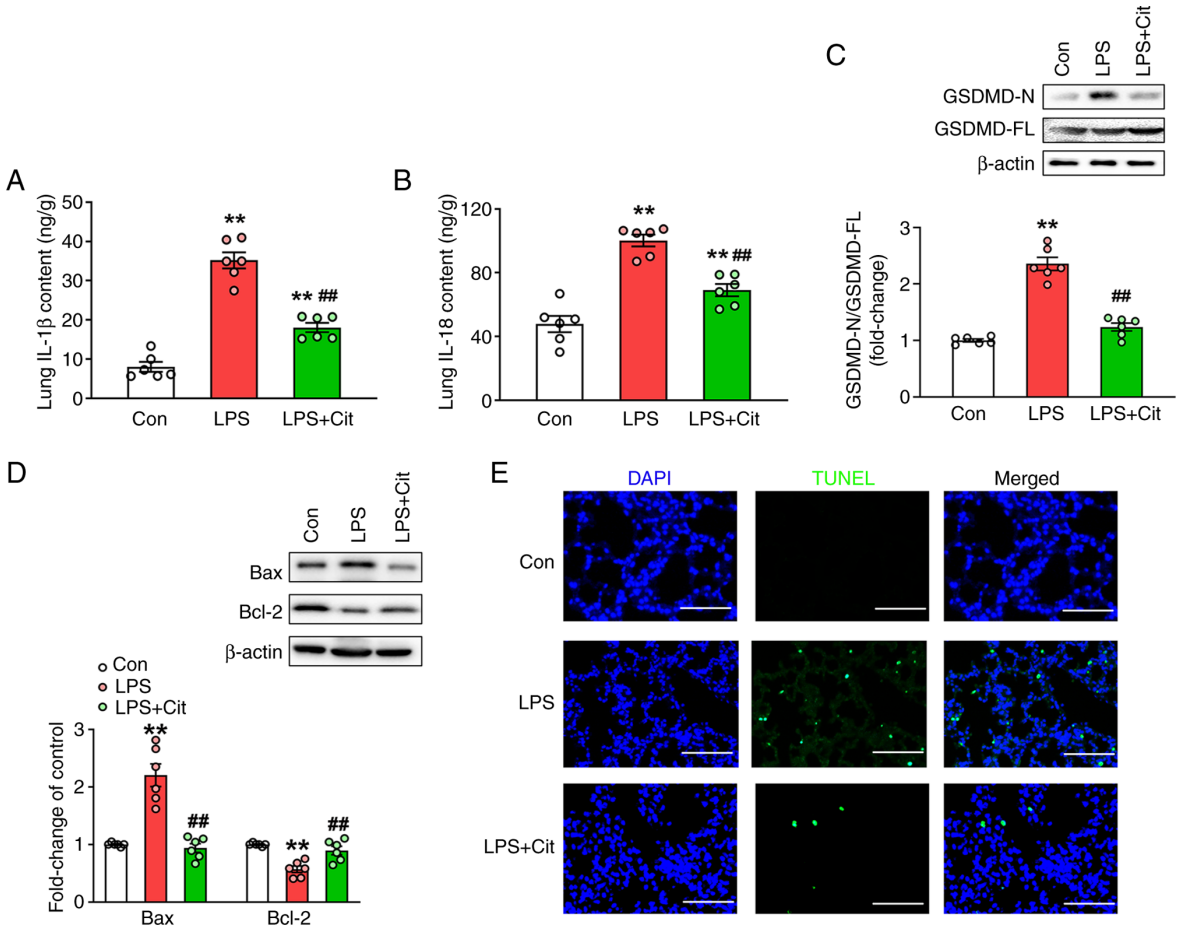

Figure 4. Cit protects against LPS-induced pulmonary pyroptosis and apoptosis. (A) IL-1β and (B) IL-18 concentration in lung tissue was determined using ELISA kits. (C) Expression of GSDMD-N was normalized to GSDMD-FL. (D) Representative western blot bands of Bax and Bcl-2. (E) Representative TUNEL-positive cells (green) in lung sections. Cell nucleus was stained with DAPI (blue). Scale bar, 100 μm. Data are expressed as the mean ± standard error of the mean (n=6). **P<0.01 vs. con; $^{\#\#}$P<0.01 vs. LPS. LPS, lipopolysaccharide; GSDMD, gasdermin D; N, N-terminal; FL, full length; Con, control; Cit, citrulline.

In the present study, NLRP3 and ASC mRNA levels, as well as NLRP3 and caspase-1 p20 cleavage fragment protein expression levels in the LPS group were significantly greater than those in the control (Fig. 3A and B). In the LPS + Cit group, levels were significantly lower than those in the LPS group (Fig. 3A and B).

Cit protects against LPS-induced pulmonary pyroptosis and apoptosis. The assembled NLRP3 inflammasome leads to the release of the pro-inflammatory cytokines IL-1β and IL-18, as well development of cell pyroptosis (30). IL-1β and IL-18 levels were significantly increased in the LPS group compared with the control (Fig. 4A-C). N-terminal region of

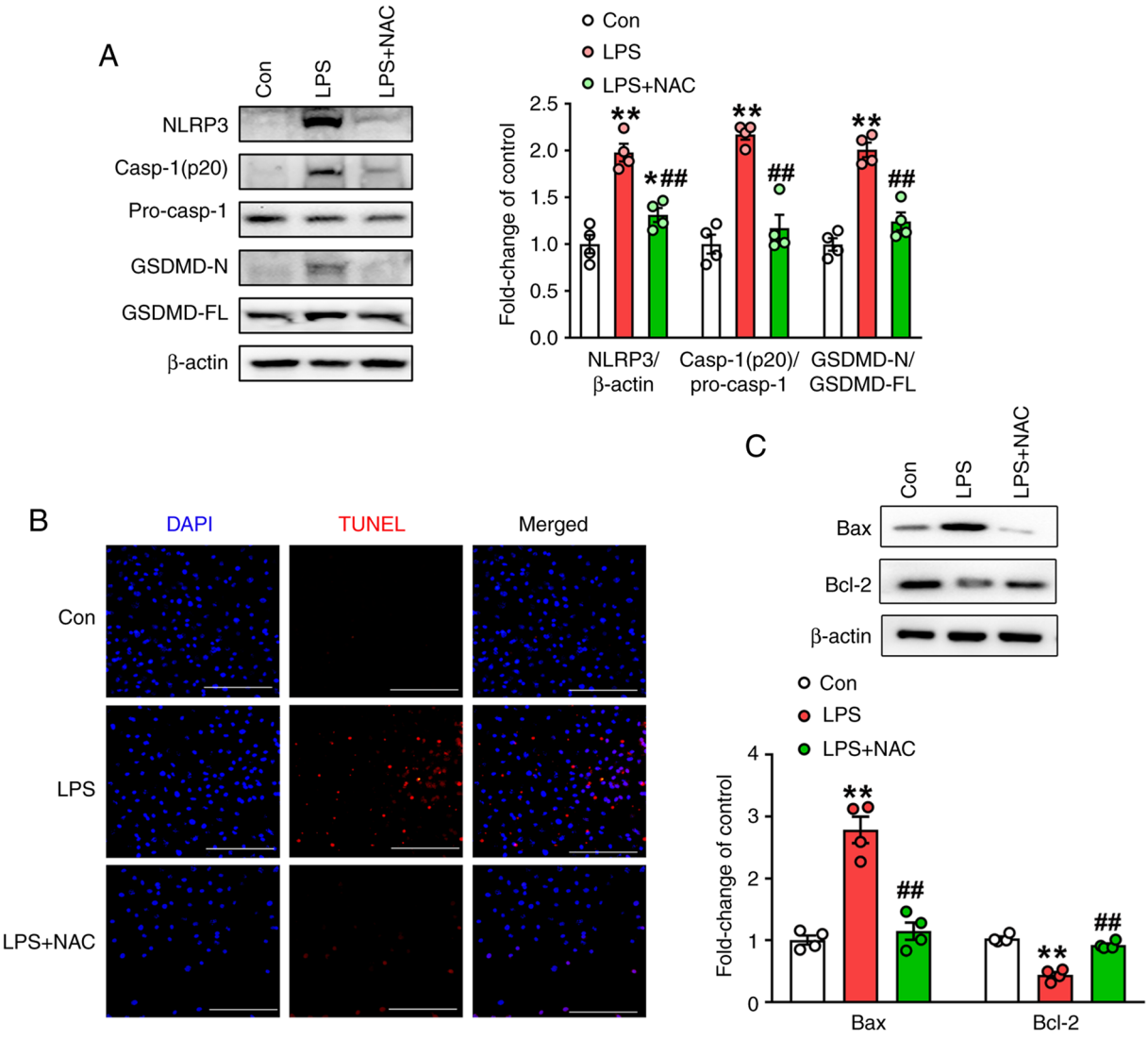

Figure 5. ROS production leads to NLRP3 inflammasome activation-mediated endothelial pyroptosis and apoptosis. Mouse pulmonary endothelial cells were exposed to LPS (1 μg/ml) in the presence or absence of the ROS scavenger NAC (5 mM) for 6 h. (A) Representative protein bands of NLRP3, casp-1(p20) and GSDMD-N. Casp-1(p20) was normalized to pro-casp-1, while GSDMD-N was normalized to GSDMD-FL. (B) Representative western blot bands of Bax and Bcl-2. (C) Representative TUNEL-positive cells (red); nuclei were counterstained with DAPI (blue). Scale bar, 100 μm. Data are expressed as the mean ± standard error of the mean (n=4). *P<0.05, **P<0.01 vs. con; $^{\#\#}$P<0.01 vs. LPS. ROS, reactive oxygen species; NLRP3, NOD-, LRR- and pyrin domain-containing protein 3; LPS, lipopolysaccharide; GSDMD-N, gasdermin D N-terminal fragment; NAC, N-acetyl-L-cysteine; FL, full length; Con, control; Cit, citrulline; ROS, reactive oxygen species; casp, caspase.

GSDMD (GSDMD-N) expression relative to the full length GSDMD (GSDMD-FL) was upregulated in the LPS group compared with the control (Fig. 4C), while in the LPS + Cit group, pretreatment with Cit significantly attenuated the effect of LPS on IL-1β and IL-18 production, as well as GSDMD-N expression (Fig. 4C). Furthermore, levels of Bcl-2, an anti-apoptotic protein, significantly decreased in the LPS group compared with the control (Fig. 4D), while the Bcl-2 expression in the LPS + Cit group was greater than in the LPS group (Fig. 4D) and comparable with the control. Consistently, levels of Bax and TUNEL-positive cells (indicative of apoptosis) were greater in the LPS group than in the control and LPS + Cit groups, while levels of these markers in LPS + Cit group were comparable with control (Fig. 4D and E). These results indicated that Cit pretreatment ameliorated LPS-induced pulmonary pyroptosis and apoptosis.

ROS production leads to NLRP3 inflammasome activation-induced endothelial pyroptosis and apoptosis. ROS participate in ALI by triggering inflammatory reactions (31). In the present study, NAC was used to inhibit activation of ROS in MLVECs to demonstrate the effect of ROS on NLRP3 activation and subsequent cell death. NAC intervention inhibited expression of the NLRP3 inflammasome and cleaved caspase-1 (Fig. 5A). Levels of TUNEL positive cells, apoptotic protein Bax and anti-apoptotic protein Bcl-2 were also reversed following inhibition of ROS (Fig. 5A-C). These findings demonstrated that the ROS scavenger NAC may decrease activation of the NLRP3 inflammasome and relieve endothelial pyroptotic and apoptotic cell death in LPS-treated MLVECs.

Cit pretreatment significantly inhibits activation of ROS and enhances the Nrf2 signaling pathway in vitro. The present study investigated the potential mechanism underlying the

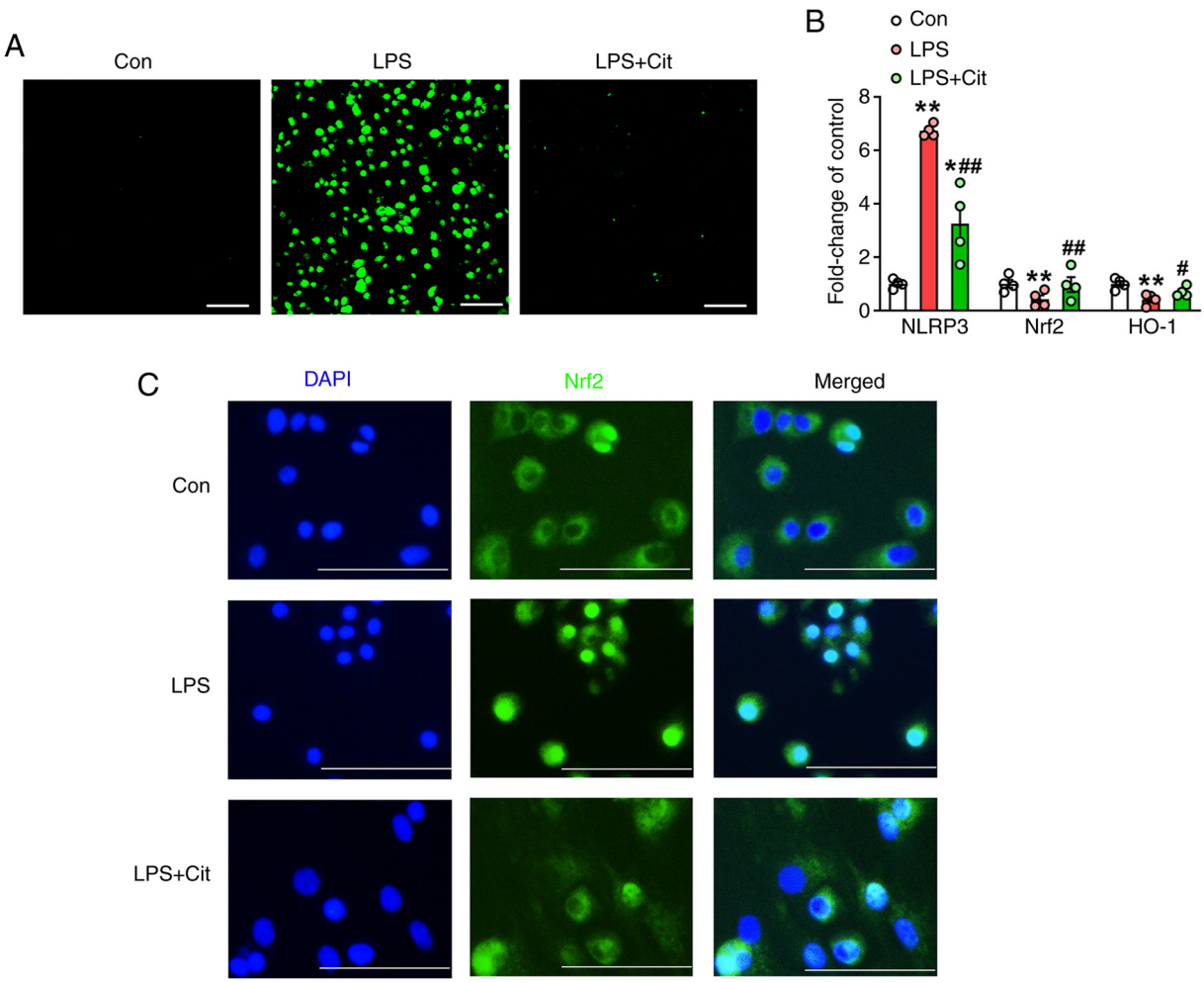

Figure 6. Cit pretreatment significantly inhibits activation of ROS and enhances the Nrf2 signaling pathway *in vitro*. (A) ROS levels were detected using 2',7'-dichlorofluorescein diacetate staining. Representative images are shown. Scale bar, 100 μm. (B) Relative mRNA levels of NOD-, LRR- and pyrin domain-containing protein 3, Nrf2 and heme oxygenase-1. Data are expressed as the mean ± SEM (n=4). *P<0.05, **P<0.01 vs. con; $^{\#}$P<0.05, $^{\#\#}$P<0.01 vs. LPS. (C) Mouse lung vascular endothelial cells were stained with Nrf2 (green), while nuclei were counterstained with DAPI (blue). Scale bar, 100 μm. ROS, reactive oxygen species; Nrf2, nuclear factor erythroid 2-related factor 2; LPS, lipopolysaccharide; Con, control; Cit, citrulline; ROS, reactive oxygen species.

protective effects of Cit. Pretreatment with Cit decreased accumulation of intracellular ROS induced by LPS (Fig. 6A). Furthermore, Cit significantly attenuated the increase in mRNA levels of NLRP3, Nrf2 and HO-1 (the primary target gene of Nrf2) induced by LPS (Fig. 6B). Immunofluorescent staining of Nrf2 showed that LPS decreased expression of Nrf2 in cytoplasm and Cit pretreatment reversed the effect of LPS (Fig. 6C).

Inhibition of Nrf2 reverses the anti-pyroptotic and anti-apoptotic effect of Cit. A specific inhibitor of Nrf2 was used to determine if the protective effect of Cit against LPS-treated MLVECs was mediated by the Nrf2 signaling pathway. In MLVECs, the effect of Cit on LPS-treated MLVECs was abrogated by Nrf2 inhibitor ML385 (5 μM), Cit pretreatment did not attenuate intracellular ROS levels induced by LPS (Fig. 7A). Inhibition of Nrf2 also blocked the protective effect of Cit against LPS-induced NLRP3 activation and pyroptosis-associated protein Casp-1(p20) and GSDMD-N (Fig. 7B). The protective effect of Cit on LPS-induced cell apoptosis was also abolished by ML385 (Fig. 7C and D). Together, these results indicated that Nrf2 was involved in the anti-pyroptotic and anti-apoptotic effect of Cit in LPS-stimulated endothelial dysfunction.

Discussion

ALI is a life-threatening disorder accompanied by high mortality (32). During the pathological process of ALI, excessive inflammatory response causes damage to organs (33). Thus, it is of importance to develop early effective interventions to prevent development of lung injury. The present results demonstrated that Cit pretreatment significantly ameliorated LPS-induced ALI and suppressed NLRP3 inflammasome expression, as well as decreased cell pyroptosis and apoptosis.

Cit exhibits biological effects, including antioxidant (34), anti-inflammatory (35) and anticancer activity (36). In rabbits, chronic L-Cit and L-Arginine supplementation abrogates state of oxidative stress in high cholesterol-induced atherosclerosis (34). In hyperoxia-induced lung injury, Cit improves alveolar and vascular growth (22). The present study confirmed the protective effect of Cit against LPS-induced NLRP3 inflammasome activation in mouse lung tissue. Furthermore, pretreatment with Cit significantly inhibited pyroptosis and

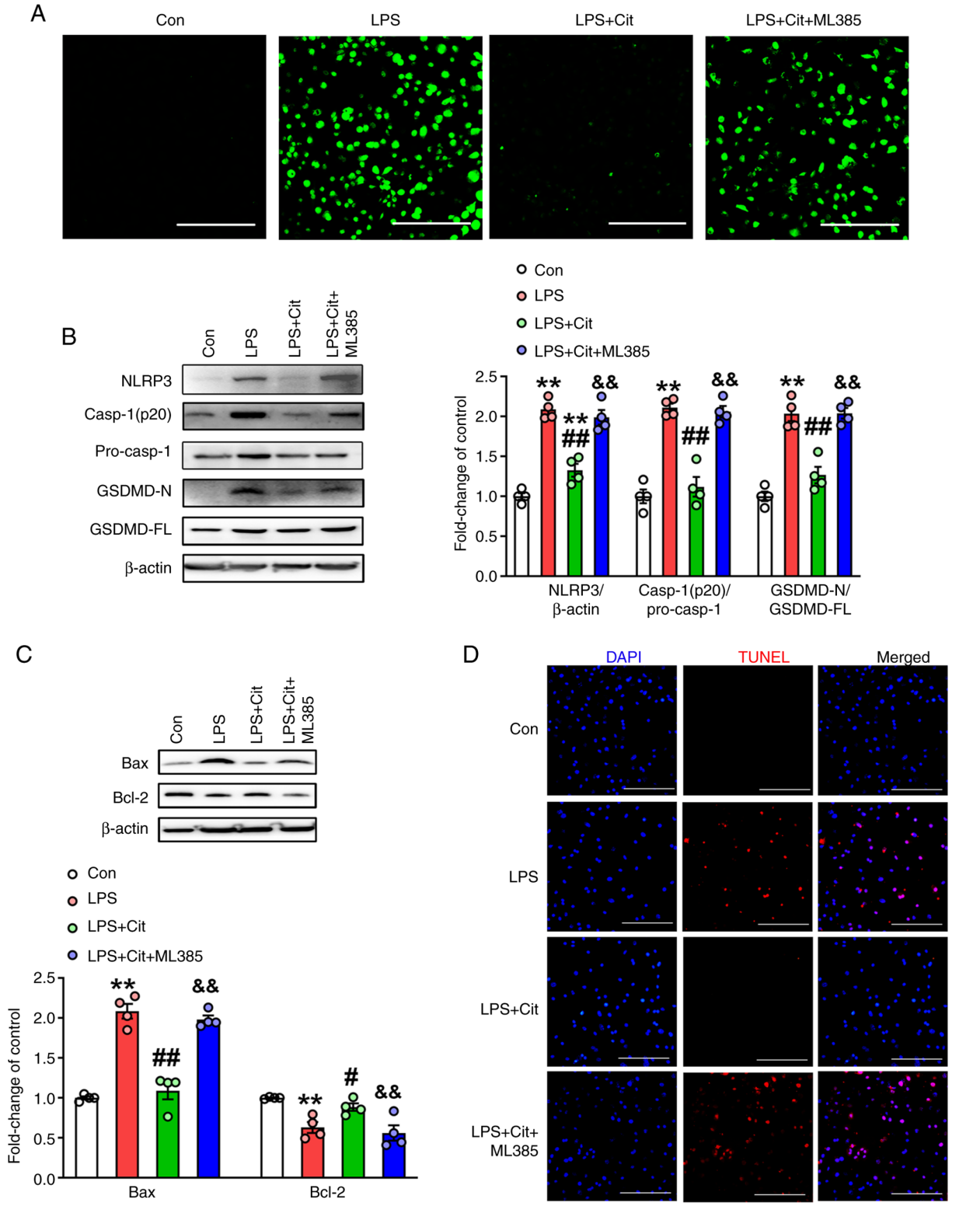

Figure 7. Inhibition of Nrf2 reverses the anti-pyroptotic and anti-apoptotic roles of Cit. Mouse lung vascular endothelial cells were exposed to LPS (1 μg/ml) and Cit with or without Nrf2 inhibitor ML138 (5 μM) pretreatment. (A) Reactive oxygen species were detected using the fluorescent probe 2',7'-dichlorofluorescein diacetate. Scale bar, 100 μm. (B) Representative western blot bands of NLRP3, casp-1(p20), GSDMD-N and (C) Bax and Bcl-2. (D) Representative TUNEL-positive cells (red). Nuclei were counterstained with DAPI (blue). Scale bar, 100 μm. Data are expressed as the mean ± standard error of the mean (n=4). **P<0.01 vs. con; $^{\#}$P<0.05 and $^{\#\#}$P<0.01 vs. LPS; $^{\&\&}$P<0.01 vs. LPS + Cit. Nrf2, nuclear factor erythroid 2-related factor 2; LPS, lipopolysaccharide; Cit, citrulline; NLRP3, NOD-, LRR- and pyrin domain-containing protein 3; Con, control; GSDMD, gasdermin D; N, N-terminal; FL, full length; casp, caspase.

apoptosis in LPS-induced ALI. Therefore, these findings suggested that multiple cell death pathways may be implicated in LPS-associated lung injury.

As previously reported, the NLRP3 inflammasome and its subsequent effectors are involved in acute and chronic lung disease (30,37). NLRP3 expression is promoted by

various stimuli, such as TNF-α and NF-κB signaling pathways and ROS (38). Cit possesses antioxidant effects. Zhou *et al* (35) found that Cit decreases histological damage in septic heart and enhances the antioxidant capacity of the heart. Previous studies showed that ROS inhibition notably decreases activation of the NLRP3 inflammasome and subsequent inflammatory reaction (31,39). Oxidative stress has been reported to promote LPS-induced endothelial injury (40). The present study detected levels of intracellular ROS and investigated their effect on NLRP3 activation. NLRP3 activation-mediated pyroptosis and apoptosis were abolished following treatment with the ROS scavenger NAC. These results demonstrated that the NLRP3 inflammasome was activated by ROS in LPS-induced endothelial dysfunction.

The present study revealed that pretreatment with Cit markedly decreased levels of ROS in LPS-induced endothelial dysfunction. Cit was shown to upregulate Nrf2 signaling and the antioxidative and downstream anti-inflammatory effects of Cit were abolished using a Nrf2 inhibitor (ML385). These findings confirmed that Nrf2 signaling was involved in the anti-inflammatory and anti-oxidative effects of Cit in LPS-induced ALI.

Overall, the present study indicated that Cit protected against LPS-induced ALI and inhibited LPS-stimulated pyroptosis and apoptosis. Cit exerted a protective role on pulmonary endothelial cells via activation of the Nrf2 signaling pathway, thereby inhibiting NLRP3 inflammasome activation due to increased levels of intracellular ROS. The results of the present study offer novel insights on the anti-inflammatory and anti-oxidative stress roles of Cit and provide a potential treatment strategy in sepsis-induced ALI. However, there were certain limitations. For example, the absence of using a specific marker of cytoplasm localization is insufficient to explain the changes of Nrf2 expression in the nucleus and cytoplasm. Further studies are needed to examine the effect of Cit on the Nrf2 signaling pathway.

Acknowledgements

Not applicable.

Funding

The present study was supported by grants from the National Natural Science Foundation of China (grant nos. 82002070 and 81901990).

Availability of data and materials

The datasets used and/or analyzed during the current study are available from the corresponding author on reasonable request.

Authors' contributions

LQY and SYL conceived the study. YX and YQZ conducted the experiments. LC, YW and ZL analyzed the data. YW and ZL wrote and revised the manuscript. LQY and SYL confirm the authenticity of all the raw data. All authors have read and approved the final manuscript.

Ethics approval and consent to participate

All animal studies were approved by the Animal Ethics Committee of Xinhua Hospital Affiliated to Shanghai Jiaotong University, School of Medicine, Shanghai, China (approval no. XHEC-NSFC-2020-038).

Patient consent for publication

Not applicable.

Competing interests

The authors declare that they have no competing interests.

References

1. Butt Y, Kurdowska A and Allen TC: Acute lung injury: A clinical and molecular review. Arch Pathol Lab Med 140: 345-350, 2016.
2. Xie W, Lu Q, Wang K, Lu J, Gu X, Zhu D, Liu F and Guo Z: miR-34b-5p inhibition attenuates lung inflammation and apoptosis in an LPS-induced acute lung injury mouse model by targeting progranulin. J Cell Physiol 233: 6615-6631, 2018.
3. Bosmann M and Ward PA: Protein-based therapies for acute lung injury: Targeting neutrophil extracellular traps. Expert Opin Ther Targets 18: 703-714, 2014.
4. Bedirli A, Kerem M, Pasaoglu H, Akyurek N, Tezcaner T, Elbeg S, Memis L and Sakrak O: Beta-glucan attenuates inflammatory cytokine release and prevents acute lung injury in an experimental model of sepsis. Shock 27: 397-401, 2007.
5. Dong Z and Yuan Y: Accelerated inflammation and oxidative stress induced by LPS in acute lung injury: Inhibition by ST1926. Int J Mol Med 41: 3405-3421, 2018.
6. Zahid A, Li B, Kombe AJK, Jin T and Tao J: Pharmacological inhibitors of the NLRP3 inflammasome. Front Immunol 10: 2538, 2019.
7. Shi J, Gao W and Shao F: Pyroptosis: Gasdermin-mediated programmed necrotic cell death. Trends Biochem Sci 42: 245-254, 2017.
8. Li DX, Wang CN, Wang Y, Ye CL, Jiang L, Zhu XY and Liu YJ: NLRP3 inflammasome-dependent pyroptosis and apoptosis in hippocampus neurons mediates depressive-like behavior in diabetic mice. Behav Brain Res 391: 112684, 2020.
9. Wang S, Zhao J, Wang H, Liang Y, Yang N and Huang Y: Blockage of P2X7 attenuates acute lung injury in mice by inhibiting NLRP3 inflammasome. Int Immunopharmacol 27: 38-45, 2015.
10. Hou L, Yang Z, Wang Z, Zhang X, Zhao Y, Yang H, Zheng B, Tian W, Wang S, He Z and Wang X: NLRP3/ASC-mediated alveolar macrophage pyroptosis enhances HMGB1 secretion in acute lung injury induced by cardiopulmonary bypass. Lab Invest 98: 1052-1064, 2018.
11. Li D, Ren W, Jiang Z and Zhu L: Regulation of the NLRP3 inflammasome and macrophage pyroptosis by the p38 MAPK signaling pathway in a mouse model of acute lung injury. Mol Med Rep 18: 4399-4409, 2018.
12. Fukumoto J, Fukumoto I, Parthasarathy PT, Cox R, Huynh B, Ramanathan GK, Venugopal RB, Allen-Gipson DS, Lockey RF and Kolliputi N: NLRP3 deletion protects from hyperoxia-induced acute lung injury. Am J Physiol Cell Physiol 305: C182-C189, 2013.
13. Jiang R, Xu J, Zhang Y, Zhu X, Liu J and Tan Y: Ligustrazine alleviate acute lung injury through suppressing pyroptosis and apoptosis of alveolar macrophages. Front Pharmacol 12: 680512, 2021.
14. Abais JM, Xia M, Zhang Y, Boini KM and Li PL: Redox regulation of NLRP3 inflammasomes: ROS as trigger or effector? Antioxid Redox Signal 22: 1111-1129, 2015.
15. MacNee W: Oxidative stress and lung inflammation in airways disease. Eur J Pharmacol 429: 195-207, 2001.
16. Ahmed SM, Luo L, Namani A, Wang XJ and Tang X: Nrf2 signaling pathway: Pivotal roles in inflammation. Biochim Biophys Acta Mol Basis Dis 1863: 585-597, 2017.
17. Ma Q: Role of nrf2 in oxidative stress and toxicity. Annu Rev Pharmacol Toxicol 53: 401-426, 2013.

18. Tkachev VO, Menshchikova EB and Zenkov NK: Mechanism of the Nrf2/Keap1/ARE signaling system. Biochemistry (Mosc) 76: 407-422, 2011.
19. Hou Y, Wang Y, He Q, Li L, Xie H, Zhao Y and Zhao J: Nrf2 inhibits NLRP3 inflammasome activation through regulating Trx1/TXNIP complex in cerebral ischemia reperfusion injury. Behav Brain Res 336: 32-39, 2018.
20. Allerton TD, Proctor DN, Stephens JM, Dugas TR, Spielmann G and Irving BA: l-Citrulline supplementation: Impact on cardiometabolic health. Nutrients 10: 291, 2018.
21. Morita M, Hayashi T, Ochiai M, Maeda M, Yamaguchi T, Ina K and Kuzuya M: Oral supplementation with a combination of L-citrulline and L-arginine rapidly increases plasma L-arginine concentration and enhances NO bioavailability. Biochem Biophys Res Commun 454: 53-57, 2014.
22. Grisafi D, Tassone E, Dedja A, Oselladore B, Masola V, Guzzardo V, Porzionato A, Salmaso R, Albertin G, Artusi C, *et al*: L-citrulline prevents alveolar and vascular derangement in a rat model of moderate hyperoxia-induced lung injury. Lung 190: 419-430, 2012.
23. National Research Council (US) Committee for the Update of the Guide for the Care and Use of Laboratory Animals. Guide for the care and use of laboratory animals. 8th edition. Washington (DC): National Academies Press (US), 2011.
24. Miyake K, Murakami T, Kiyuna T, Igarashi K, Kawaguchi K, Miyake M, Li Y, Nelson SD, Dry SM, Bouvet M, *et al*: The combination of temozolomide-irinotecan regresses a doxorubicin-resistant patient-derived orthotopic xenograft (PDOX) nude-mouse model of recurrent Ewing's sarcoma with a FUS-ERG fusion and CDKN2A deletion: Direction for third-line patient therapy. Oncotarget 8: 103129-103136, 2017.
25. Wang Y, Gao TT, Xu DF, Zhu XY, Dong WW, Lv Z, Liu YJ and Jiang L: Upregulation of sphingosine kinase 1 contributes to ventilator-associated lung injury in a two-hit model. Int J Mol Med 44: 2077-2090, 2019.
26. Wang Y, Liu YJ, Xu DF, Zhang H, Xu CF, Mao YF, Lv Z, Zhu XY and Jiang L: DRD1 downregulation contributes to mechanical stretch-induced lung endothelial barrier dysfunction. Theranostics 11: 2505-2521, 2021.
27. Dong WW, Liu YJ, Lv Z, Mao YF, Wang YW, Zhu XY and Jiang L: Lung endothelial barrier protection by resveratrol involves inhibition of HMGB1 release and HMGB1-induced mitochondrial oxidative damage via an Nrf2-dependent mechanism. Free Radic Biol Med 88: 404-416, 2015.
28. Livak KJ and Schmittgen TD: Analysis of relative gene expression data using real-time quantitative PCR and the 2(-Delta Delta C(T)) method. Methods 25: 402-408, 2001.
29. Yang H, Lv H, Li H, Ci X and Peng L: Oridonin protects LPS-induced acute lung injury by modulating Nrf2-mediated oxidative stress and Nrf2-independent NLRP3 and NF-κB pathways. Cell Commun Signal 17: 62, 2019.
30. Lv Z, Wang Y, Liu YJ, Mao YF, Dong WW, Ding ZN, Meng GX, Jiang L and Zhu XY: NLRP3 inflammasome activation contributes to mechanical stretch-induced endothelial-mesenchymal transition and pulmonary fibrosis. Crit Care Med 46: e49-e58, 2018.
31. Han S, Cai W, Yang X, Jia Y, Zheng Z, Wang H, Li J, Li Y, Gao J, Fan L and Hu D: ROS-mediated NLRP3 inflammasome activity is essential for burn-induced acute lung injury. Mediators Inflamm 2015: 720457, 2015.
32. Lv X, Lu X, Zhu J and Wang Q: Lipopolysaccharide-induced acute lung injury is associated with increased ran-binding protein in microtubule-organizing center (RanBPM) molecule expression and mitochondria-mediated apoptosis signaling pathway in a mouse model. Med Sci Monit 26: e923172, 2020.
33. Liu S, Su X, Pan P, Zhang L, Hu Y, Tan H, Wu D, Liu B, Li H, Li H, *et al*: Neutrophil extracellular traps are indirectly triggered by lipopolysaccharide and contribute to acute lung injury. Sci Rep 6: 37252, 2016.
34. Hayashi T, Juliet PA, Matsui-Hirai H, Miyazaki A, Fukatsu A, Funami J, Iguchi A and Ignarro LJ: l-Citrulline and l-arginine supplementation retards the progression of high-cholesterol-diet-induced atherosclerosis in rabbits. Proc Natl Acad Sci USA 102: 13681-13686, 2005.
35. Zhou JQ, Xu X, Zhen WW, Luo YL, Cai B and Zhang S: Protective effect of citrulline on the hearts of rats with sepsis induced by cecal ligation and puncture. Biomed Res Int 2018: 2574501, 2018.
36. Ouaknine Krief J, Helly de Tauriers P, Dumenil C, Neveux N, Dumoulin J, Giraud V, Labrune S, Tisserand J, Julie C, Emile JF, *et al*: Role of antibiotic use, plasma citrulline and blood microbiome in advanced non-small cell lung cancer patients treated with nivolumab. J Immunother Cancer 7: 176, 2019.
37. Sohn SH, Lee JM, Park S, Yoo H, Kang JW, Shin D, Jung KH, Lee YS, Cho J and Bae H: The inflammasome accelerates radiation-induced lung inflammation and fibrosis in mice. Environ Toxicol Pharmacol 39: 917-926, 2015.
38. Latz E, Xiao TS and Stutz A: Activation and regulation of the inflammasomes. Nat Rev Immunol 13: 397-411, 2013.
39. Shirasuna K, Usui F, Karasawa T, Kimura H, Kawashima A, Mizukami H, Ohkuchi A, Nishimura S, Sagara J, Noda T, *et al*: Nanosilica-induced placental inflammation and pregnancy complications: Different roles of the inflammasome components NLRP3 and ASC. Nanotoxicology 9: 554-567, 2015.
40. Liang CF, Liu JT, Wang Y, Xu A and Vanhoutte PM: Toll-like receptor 4 mutation protects obese mice against endothelial dysfunction by decreasing NADPH oxidase isoforms 1 and 4. Arterioscler Thromb Vasc Biol 33: 777-784, 2013.

This work is licensed under a Creative Commons Attribution-NonCommercial-NoDerivatives 4.0 International (CC BY-NC-ND 4.0) License.